

BEYOND THE BOUNDARIES OF PROXIMAL POLICY OPTIMIZATION

Charlie B. Tan¹ Edan Toledo^{2,3} Benjamin Ellis¹ Jakob N. Foerster¹ Ferenc Huszár⁴

¹University of Oxford ²University College London ³Meta ⁴University of Cambridge

ABSTRACT

Proximal policy optimization (PPO) is a widely-used algorithm for on-policy reinforcement learning. This work offers an alternative perspective of PPO, in which it is decomposed into the inner-loop *estimation* of update vectors, and the outer-loop *application* of updates using gradient ascent with unity learning rate. Using this insight we propose *outer proximal policy optimization* (outer-PPO); a framework wherein these update vectors are applied using an arbitrary gradient-based optimizer. The decoupling of update estimation and update application enabled by outer-PPO highlights several implicit design choices in PPO that we challenge through empirical investigation. In particular we consider non-unity learning rates and momentum applied to the outer loop, and a momentum-bias applied to the inner estimation loop. Methods are evaluated against an aggressively tuned PPO baseline on Brax, Jumanji and MinAtar environments; non-unity learning rates and momentum both achieve statistically significant improvement on Brax and Jumanji, given the same hyperparameter tuning budget.

1 INTRODUCTION

Proximal policy optimization (PPO) (Schulman et al., 2017b) is ubiquitous within modern reinforcement learning (RL), having found success in domains such as robotics (Andrychowicz et al., 2020b), gameplay (Berner et al., 2019), and research applications (Mirhoseini et al., 2021). Given its ubiquity, significant research effort has explored the theoretical (Hsu et al., 2020; Kuba et al., 2022) and empirical (Engstrom et al., 2020; Andrychowicz et al., 2020a) properties of PPO.

PPO is an on-policy algorithm; at each iteration it collects a dataset using the current (behavior) policy. This dataset is used to construct a surrogate to the true objective, enabling gradient-based optimization while seeking to prevent large changes in policy between iterations, similar to trust region policy optimization (Schulman et al., 2017a). The solution to the surrogate objective is then taken as the behavior parameters for the following iteration, defining the behavior policy with which to collect the following dataset. The behavior policies are therefore *exactly coupled* with the preceding surrogate objective solution.

In this work we instead consider the inner-loop optimization of each surrogate objective to estimate an update vector, which we name the *outer gradient*. A trivial result follows that the outer loop of PPO can be viewed to update the behavior parameters using unity learning rate $\sigma = 1$ gradient ascent on the outer gradients. Using this insight we propose outer-PPO, a novel variation of PPO that employs an arbitrary gradient-based optimizer in the outer loop of PPO. Outer-PPO *decouples* the estimation and application of updates in way not possible in standard PPO. An illustration of outer-PPO applying a learning rate greater than unity is provided in figure 1. The new behaviors enabled by outer-PPO raise several questions related to implicit design choices of PPO:

Question 1. *Is the unity learning rate always optimal?*

Question 2. *Is the independence (lack of prior trajectory information e.g momentum) of each outer update step always optimal?*

Question 3. *Is initializing the inner loop surrogate objective optimization at the behavior parameters (without exploiting prior trajectory / momentum) always optimal?*

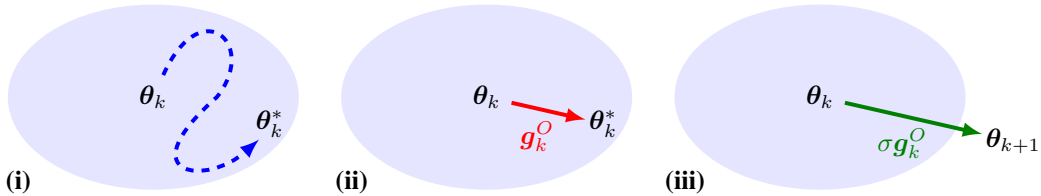


Figure 1: **Diagram of outer-PPO estimating and applying the outer gradient as an update.** (i) Transitions are collected with policy $\pi(\theta_k)$ defining a surrogate objective and corresponding ‘trust-region’ (shaded) surrounding θ_k ; inner-loop optimization of the surrogate objective (blue dashed) yields θ_k^* . (ii) Outer-PPO computes outer gradient as $g_k^O \leftarrow \theta_k^* - \theta_k$. (iii) Outer-PPO updates behavior parameters using an arbitrary gradient based optimizer applied to the outer gradient to give θ_{k+1} , in this case gradient ascent with a learning rate $\sigma > 1$. Standard PPO can be understood as directly taking $\theta_{k+1} \leftarrow \theta_k^*$, or as a special case of outer-PPO corresponding to gradient ascent with learning rate $\sigma = 1$.

This work forms an empirical investigation of the aforementioned questions. To motivate this investigation, consider the clipping parameter ϵ of PPO, controlling the size of the ‘trust region’ within which we seek to restrict our update. If ϵ is set too low, we restrict ourselves to small policy updates. Conversely, if we set ϵ too high we decrease the reliability of our update direction. In outer-PPO, introducing an outer learning rate decouples these two effects; we are able to reliably estimate an update vector using a moderate ϵ , but then take step of large magnitude in this direction.

We emphasize that we do not seek to identify the most performant configuration possible but to understand the performance of outer-PPO relative to a well-tuned PPO baseline. To this end we restrict the tuning of outer-PPO to simple grid searches applied to fixed base PPO hyperparameters.

Our contributions are as follows:

- We propose *outer proximal policy optimization* (outer-PPO), in which an arbitrary gradient-based optimizer is applied to the ‘outer gradients’ of PPO. By tracking the outer trajectory, outer-PPO further permits a momentum bias to be applied to the inner-loop initialization.
- We optimize a PPO baseline through extensive hyperparameter sweeps (total of 38,400 agent trained) on subsets of Brax (6 tasks) (Freeman et al., 2021), Jumanji (4 tasks) (Bonnet et al., 2024), and MinAtar (4 tasks) (Young & Tian, 2019). We open-source the sweep database files to facilitate future research against strongly tuned baselines.
- We perform three lightweight outer-PPO grid searches on non-unity outer learning rates, outer Nesterov momentum and biased-initialization, each addressing questions 1, 2 and 3 respectively.
- We evaluate the outer-PPO methods against the baseline, using 64 seeds per task over the 14 different tasks. We find non-unity outer learning rates to yield the greatest improvement (5-10%) on both Brax and Jumanji. Outer Nesterov also improves performance on Brax and Jumanji. Biased initialization achieves a moderate improvement on Jumanji alone. No method improves over the baseline on MinAtar.
- Given the stated empirical results we conclude the *negative* for questions 1, 2 and 3. Relaxing each of these PPO design choices can lead to consistent, statistically significant improvement of performance over at least one of the evaluated environment suites.
- We propose that practitioners able to experiment may explore non-unity outer learning rates given the simplicity (single hyperparameter) and consistent improvement achieved on Brax and Jumanji.

2 BACKGROUND

2.1 REINFORCEMENT LEARNING

We consider the standard reinforcement learning formulation of a Markov decision process $\mathcal{M} = \langle \mathcal{S}, \mathcal{A}, \mathcal{T}, r, \gamma \rangle$, where \mathcal{S} is the set of states, \mathcal{A} is the set of actions, $\mathcal{T} : \mathcal{S} \times \mathcal{A} \rightarrow \Delta(\mathcal{S})$ is the state transition probability function, $r : \mathcal{S} \times \mathcal{A} \rightarrow \Delta(\mathbb{R})$ is the reward function, and $\gamma \in [0, 1]$ is the discount factor. We use the notation $\Delta(\mathbf{X})$ to denote the probability distribution over a set \mathbf{X} . The reinforcement learning objective is to maximize the expected return $\mathbb{E}_\pi[G_t] = \mathbb{E}_\pi[\sum_t \gamma^t r_t]$ given a *policy* $\pi : \mathcal{S} \rightarrow \Delta(\mathcal{A})$ defining the agent behavior. In actor-critic policy optimization the policy is explicitly represented as a parametric function $\pi : \mathcal{S} \times \boldsymbol{\theta}^\pi \rightarrow \Delta(\mathcal{A})$, and a *value function* $V : \mathcal{S} \times \boldsymbol{\theta}^V \rightarrow \mathbb{R}$ is employed to guide optimization. In deep RL (Mnih et al., 2015; Silver et al., 2017) neural networks are used for the policy and value functions, for ease of notation we consider $\boldsymbol{\theta} \in \mathbb{R}^{(d_\pi + d_V)}$ as the concatenation of the respective weight vectors.

2.2 PROXIMAL POLICY OPTIMIZATION

Proximal policy optimization was proposed by Schulman et al. (2017b), and has since become one of the most popular algorithms for on-policy reinforcement learning. At each iteration k a dataset of transitions \mathcal{D}_k is collected using policy $\pi(\boldsymbol{\theta}_k)$, and advantages \hat{A}_k are estimated using generalized advantage estimation (GAE) (Schulman et al., 2018). The transition dataset and advantages are then used within an inner optimization loop, in which the policy parameters $\boldsymbol{\theta}^\pi$ are optimized with respect to a given surrogate objective along with the value parameters $\boldsymbol{\theta}^V$. Pseudocode for a single iteration of PPO is provided in algorithm 1, where INNEROPTIMIZATIONLOOP is defined in appendix A. The full algorithm updates parameters iteratively by $\boldsymbol{\theta}_{k+1} \leftarrow \text{PPOITERATION}(\boldsymbol{\theta}_k)$.

Algorithm 1 Proximal policy optimization iteration

- 1: **function** PPOITERATION($\boldsymbol{\theta}$)
 - 2: Collect set of trajectories \mathcal{D} by running policy $\pi(\boldsymbol{\theta})$
 - 3: Estimate advantages \hat{A} with GAE.
 - 4: $\boldsymbol{\theta}^* \leftarrow \text{INNEROPTIMIZATIONLOOP}(\boldsymbol{\theta}, \mathcal{D}, \hat{A})$
 - 5: **return** $\boldsymbol{\theta}^*$
 - 6: **end function**
-

PPO permits the use of any arbitrary surrogate objective, though it is most commonly associated with the *clipped objective* Schulman et al. (2017b) stated in equation 1.

$$L^\pi(\boldsymbol{\theta}^\pi) = \mathbb{E}_{s, a \sim \mathcal{D}_k} \left[\min \left(\rho(\boldsymbol{\theta}^\pi) \hat{A}, \text{clip}(\rho(\boldsymbol{\theta}^\pi), 1 - \epsilon, 1 + \epsilon) \hat{A} \right) \right] \quad (1)$$

Here $\rho(\boldsymbol{\theta}^\pi) = \frac{\pi(a|s)}{\pi_k(a|s)}$ is the ratio between our current policy π and the behavior policy π_k , and ϵ is the clipping threshold. The value function is similarly optimized using either simple regression. $L^V(\boldsymbol{\theta}^V) = (V_{\boldsymbol{\theta}_k} - V_{\text{targ}})^2$ or the clipped objective defined in appendix A.

2.3 TRUST REGIONS

A *trust region* is a region surrounding an optimization iterate $\boldsymbol{\theta}_k$ within which we permit our algorithm to update the parameters to $\boldsymbol{\theta}_{k+1}$. In TRPO, a trust region surrounding the behavior parameters is explicitly defined as the region in parameter space $\boldsymbol{\theta} \in \Theta$ satisfying $\mathbb{E}_{s \sim \mathcal{D}_k} [D_{\text{KL}}(\pi(\boldsymbol{\theta}_k|s) \parallel \pi(\boldsymbol{\theta}|s))] \leq \delta$. Optimizing subject to this constraint prevents large changes in the policy between successive iterations, and gives rise to a guarantee of *monotonic improvement*. Similarly, if the clipped surrogate objective of PPO is replaced with a KL penalty $L^\pi(\boldsymbol{\theta}) = \mathbb{E}_{s, a \sim \mathcal{D}_k} [\rho(\boldsymbol{\theta}) \hat{A} - \beta D_{\text{KL}}(\pi(\boldsymbol{\theta}_k|s) \parallel \pi(\boldsymbol{\theta}|s))]$, a trust-region is implicitly defined for some δ . Both TRPO and PPO-KL approximate the natural policy gradient (Kakade, 2001), (Hsu et al., 2020); the steepest direction in the non-Euclidean geometry of policy space induced by the Fisher information metric.

Unlike the KL penalized surrogate, the clipped surrogate objective of equation 1 *does not* define a formal trust region. We can however define the region of non-zero gradients, with gradient defined as in equation 2.

$$\nabla_{\theta^\pi} L^\pi(\theta^\pi) = \mathbb{E}_{s, a \sim \mathcal{D}_k} \left[\hat{A} \nabla_{\theta^\pi} \rho(\theta^\pi) \cdot \mathbb{I} \left(|\rho(\theta^\pi) - 1| \leq \epsilon \text{ or } (\rho(\theta^\pi) - 1) \hat{A} \leq 0 \right) \right] \quad (2)$$

Here $\mathbb{I}(\cdot)$ is an indicator function that equals 1 if and only if the argument is true, and 0 otherwise. Whilst the subspace $\nabla_{\theta} L^\pi > 0$ can be considered analogous to a trust region, it is possible to irreversibly step arbitrarily far beyond this region (Hsu et al., 2020). Nonetheless, where not ambiguous we shall abuse notation and refer to $\nabla_{\theta} L^\pi > 0$ as the trust region of the clipped surrogate. Whilst not defining a formal trust region, the clipped objective enjoys theoretical motivation as a valid drift function in the mirror learning framework (Kuba et al., 2022), hence also benefits from monotonic improvement and convergence guarantees.

3 OUTER-PPO

In equation 3 we define the outer gradient of PPO.

$$\mathbf{g}^O(\theta) = \text{PPOITERATION}(\theta) - \theta \quad (3)$$

The behavior parameter update of PPO $\theta_{k+1} \leftarrow \text{PPOITERATION}(\theta_k)$ can now be equivalently expressed as $\theta_{k+1} \leftarrow \theta_k + \mathbf{g}^O(\theta_k)$. Evidently, PPO is exactly gradient ascent, with a constant learning rate $\sigma = 1$, on its outer gradients. With this simple result established, we propose a family of methods employing arbitrary optimizers on the PPO outer loop, denoted as *outer-PPO*. As an illustrating example, a comparison of standard PPO and outer-PPO with non-unity learning rates is provided in algorithms 2 and 3. We additionally propose a closely-related method for biasing the inner estimation loop using the prior (outer) trajectory, denoted as *biased initialization*.

3.1 OUTER LEARNING RATES

Varying the outer learning rate scales the update applied to the behavior parameters, as defined in algorithm 3 and illustrated in figure 1. The behavior of scaling the outer gradient can not be directly recovered by varying the PPO hyperparameters.

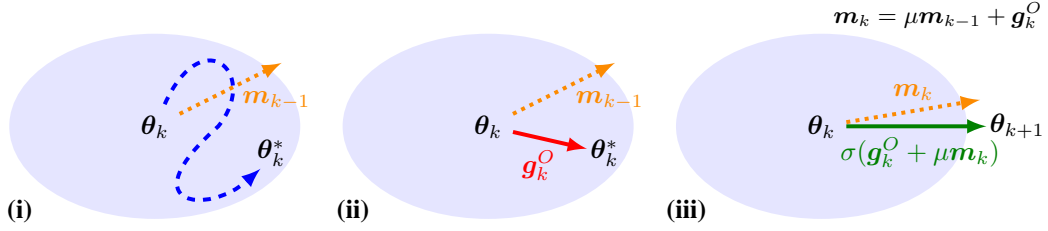
Algorithm 2 Standard PPO

Input: θ_0 (parameters)
 1: **for** $k = 0, 1, 2, \dots$ **do**
 2: $\theta^* \leftarrow \text{PPOITERATION}(\theta_k)$
 3: $\theta_{k+1} \leftarrow \theta^*$
 4: **end for**

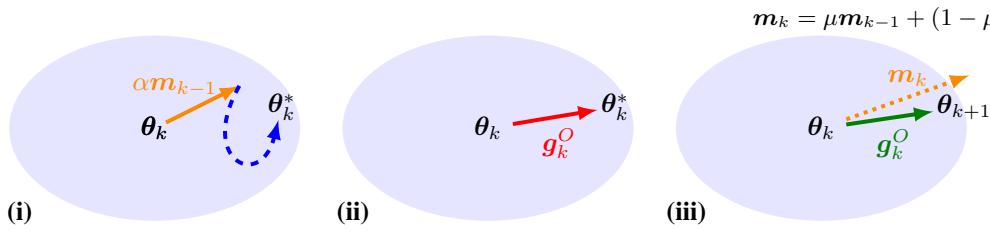
Algorithm 3 Outer-LR PPO

Input: θ_0 (parameters), σ (outer learning rate)
 1: **for** $k = 0, 1, 2, \dots$ **do**
 2: $\mathbf{g}_k^O \leftarrow \text{PPOITERATION}(\theta_k) - \theta_k$
 3: $\theta_{k+1} \leftarrow \theta_k + \sigma \mathbf{g}_k^O$
 4: **end for**

An outer learning rate $\sigma < 1$ interpolates between the behavior parameters θ_k and inner-loop solution θ_k^* , encoding a lack of trust in the outer gradient estimation. Whilst the magnitude of the outer gradient can be reduced by varying hyperparameters, such as the clipping ϵ or number of inner loop iterations, the outer gradients are inherently noisy due to stochastic data collection and inner-loop optimization. PPO is additionally able to irreversibly escape its clipping boundary (Engstrom et al., 2020), and can drift far from the behavior policy given sub-optimal surrogate objective parameters. These effects motivate the exploration of methods that attenuate the outer updates, irrespective of the outer gradient magnitude. In contrast, a learning rate $\sigma > 1$ amplifies the update vector, encoding confidence in its direction. Whilst the outer gradient magnitude could be increased by varying the PPO hyperparameters, in particular ϵ , increasing the size of the trust region may lead the policy to drift to beyond the region of policy space where the dataset \mathcal{D}_k collected with policy π_k can be considered representative of the environment dynamics, motivating the amplification of well-estimated outer gradients over increases to trust region size.



(a) **Outer-Nesterov PPO.** At each iteration Outer-Nesterov PPO estimates an outer gradient g_k^O , updates the momentum m_k , and steps the parameters using the Nesterov momentum update. The momentum step therefore *precedes* the construction of the following trust region, since it defines the following behavior policy $\pi(\theta_{k+1})$.



(b) **Biased initialization.** Each iteration commences with a momentum step (solid orange); the inner optimization (blue dashed) is therefore initialized at $\theta_k + \alpha m_{k-1}$. The momentum step therefore *occurs within* the trust region as the dataset \mathcal{D}_k was collected prior, and the surrogate objective remains defined relative to $\pi(\theta_k)$.

Figure 2: Comparison of Nesterov-PPO and biased initialization.

3.2 MOMENTUM

Whilst permitting novel behavior, outer-LR PPO still only exploits information from a single PPO iteration when updating the parameters. Applying momentum breaks this design choice; instead of directly updating the parameters with the scaled outer gradient σg_k^O , we update using the Nesterov momentum rule as in algorithm 4 and illustrated in figure 2a.

Algorithm 4 Outer-Nesterov PPO

- 1: Input: θ_0 (parameters), σ (learning rate), μ (momentum factor)
 - 2: $m_0 \leftarrow \mathbf{0} \in \mathbb{R}^d$
 - 3: **for** $k = 0, 1, 2, \dots$ **do**
 - 4: $g_k^O \leftarrow \text{PPOITERATION}(\theta_k) - \theta_k$
 - 5: $m_k \leftarrow \mu m_{k-1} + g_k^O$
 - 6: $\theta_{k+1} \leftarrow \theta_k + \sigma(m_k + \mu g_k^O)$
 - 7: **end for**
-

In supervised learning momentum is motivated using pathological curvature, and the ability to ‘build up speed’ (Sutskever et al., 2013). Given that the outer gradient is the solution to a surrogate objective, we do not anticipate pathological curvature presenting to the outer optimizer. However, similar to learning rates $\sigma > 1$ the increase in effective learning rate of momentum may assist in learning. Momentum can also be motivated here using resilience to noise; since any given collected dataset will be noisy, the outer gradient is also noisy. As using a learning rate $\sigma < 1$ corresponded to a lack of trust in any given outer gradient, using momentum corresponds to a smoothing process, where we at no point solely trust a single outer gradient to be accurate.

3.3 BIASED INITIALIZATION

Outer-PPO Nesterov applies a momentum-based update to the outer loop of PPO. This update occurs *before* the successive iteration’s dataset \mathcal{D}_{k+1} is collected, hence the momentum directly determines

the behavior parameters π_{k+1} for the following surrogate objective. Beyond the effects of stateful inner-loop optimizers such as Adam (Kingma & Ba, 2014), each outer gradient estimation is independent of the prior trajectory. In contrast we propose biased initialization to apply an outer momentum-based update *after* data is collected, hence *inside* the following trust region problem as in algorithm 5, where $\mathbf{m}_k = \mu\mathbf{m}_{k-1} + (1 - \mu)\mathbf{g}_k^O$ is the momentum vector, and in figure 2b.

Algorithm 5 PPO iteration with biased initialization

```

1: function BIASEDPPOITERATION( $\theta, \mathbf{m}, \alpha$ )
2:   Collect set of trajectories  $\mathcal{D}$  by running policy  $\pi(\theta)$ 
3:   Compute advantages  $\hat{A}$ .
4:    $\theta \leftarrow \theta + \alpha\mathbf{m}$ 
5:    $\theta^* \leftarrow \text{INNEROPTIMIZATIONLOOP}(\theta, \mathcal{D}, \hat{A})$ 
6:   return  $\theta^*$ 
7: end function

```

Biased initialization bears a strong similarity to the conjugate gradient initialization employed in Hessian-free optimization (Martens, 2010). The primary motivation for such techniques would be to better estimate the update vector in a given budget of inner-loop iterations.

4 EXPERIMENTS

4.1 EVALUATION PROCEDURE

We experiment on subsets of the Brax (Freeman et al., 2021), Jumanji (Bonnet et al., 2024), and MinAtar (Young & Tian, 2019) environment suites, selected as diverse examples of continuous and discrete control problems. We employ the absolute evaluation procedure recommended by Colas et al. (2018) and Gorsane et al. (2022). Absolute evaluation entails intermediate evaluations during training and a final, large-scale evaluation using the best policy identified to give the ‘absolute’ performance. We train with a budget of 1×10^7 transitions, perform 20 intermediate evaluations, and conduct final evaluation using 1280 episodes.

Recognizing the hyperparameter sensitivity of deep reinforcement learning (Hsu et al., 2020; Engstrom et al., 2020; Andrychowicz et al., 2020a), we commit significant resources to establishing a strong PPO baseline and fair evaluation. We sweep for a budget of 600 trials per task using the tree-structured Parzen estimator (Bergstra et al., 2011; Watanabe, 2023). Each trial is the mean of 4 agents, trained using seeds randomly sampled from $[0, 10000]$, for a total of 2400 agents trained per task during baseline tuning. A total of 11 hyperparameters are tuned, each with extensive ranges considered. Full descriptions of the hyperparameter sweep ranges, and the optimal values identified are provided in appendix C.

After hyperparameter tuning a final 64 agents are trained per environment task, where the set of evaluation seeds is non-overlapping with seeds used for hyperparameter tuning. To compare methods we aggregate performance over the tasks of an environment suite following the procedure recommended by Agarwal et al. (2021), normalizing with the min/max return found for each task across all trained agents (including sweep agents), a table of which is presented in appendix D.

4.2 DEFINED EXPERIMENTS

We consider the three outer-PPO methods defined in section 3; outer-LR, outer-Nesterov and biased initialization, addressing questions 1, 2, and 3 respectively. The outer-PPO methods are grid searched using increments of 0.1 for all hyperparameters. Outer-LR has a single hyperparameter; outer learning rate σ , which is swept over the range $[0.1, 4.0]$ (40 trials). Nesterov-PPO two hyperparameters; σ $[0.1, 1.0]$ and momentum factor μ $[0.1, 0.9]$ (90 trials). Biased initialization also has two hyperparameters; bias learning rate α $[0.1, 1.0]$, bias momentum μ $[0.0, 0.9]$ (100 trials). The base PPO hyperparameters are frozen from the baseline sweep up to the 500th trial, such that no method is tuned using a budget greater than the 600 trials used by the baseline. The optimal hyperparameters identified for each sweep are provided in the figures of appendix E.

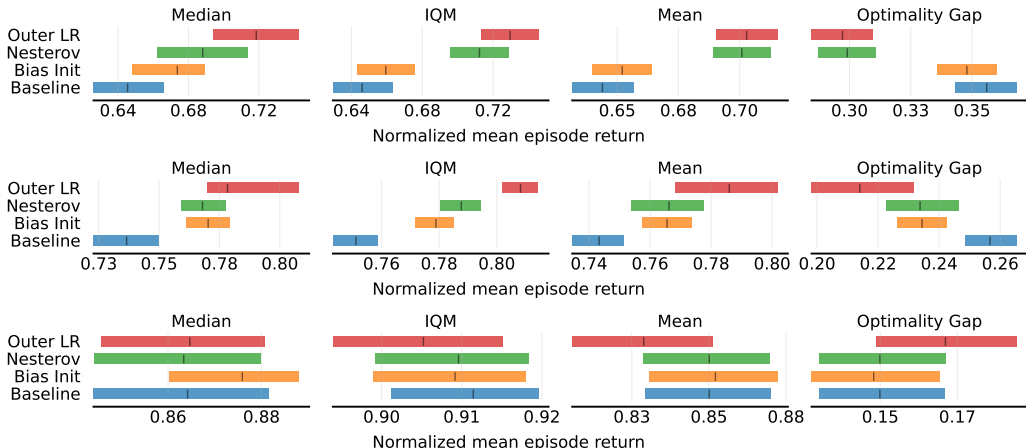


Figure 3: **Aggregate point estimates** for Brax (upper), Jumanji (center), and MinAtar (lower). Optimal hyperparameters *per-environment* are used. Normalized to task min/max across all experiments.

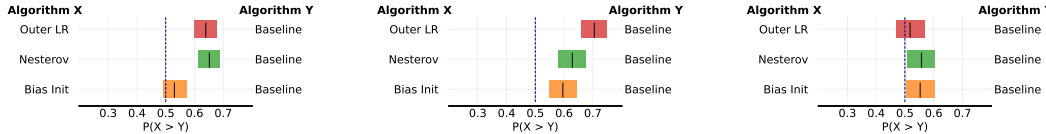


Figure 4: **Probability of improvement** for Brax (left), Jumanji (center), and MinAtar (right). Optimal hyperparameters *per-environment* are used. Normalized to task min/max across all experiments.

5 RESULTS

5.1 EMPIRICAL PERFORMANCE

We first consider the performance of the three outer-PPO methods, where the optimal hyperparameters identified from the grid sweeps *per-environment* are employed. In figures 3 and 4 we present the aggregate point estimates and probability of improvement. Further results including sample efficiency curves are provided in appendix D.

Aggregate point estimates. Outer-LR demonstrates a statistically significant improvement over the PPO baseline on Brax and Jumanji for all point estimates considered (median, IQM, mean, optimality gap). Outer-Nesterov also demonstrates enhanced performance on Brax and Jumanji; this improvement is less substantial than that of outer-LR but remains statistically significant on all point estimates aside from the Brax median. Biased initialization is the weakest of the outer-PPO instantiations, with minor improvements lacking statistical significance on Brax and moderate but significant improvements on Jumanji. No method improves over baseline on MinAtar.

Probability of improvement. All methods have a probability of improvement (over baseline) greater than 0.5. In most cases this improvement is statistically significant, aside from biased initialization on Brax and outer-LR on MinAtar. Notably, outer-LR has a probability of improvement greater than 0.6 on Brax and greater than 0.7 on Jumanji.

5.2 HYPERPARAMETER SENSITIVITY

In the results of figures 3 and 4, the optimal hyperparameters from each *per-environment* outer-PPO grid search are used. We now consider the sensitivity of outer-PPO to these hyperparameters. In figures 5, 6, and 7 we present the return, *normalized across each environment suite*, as a function of the sweep hyperparameters for outer-LR, outer-Nesterov and biased initialization. Normalization is again performed using the extreme values presented in appendix D. Analogous plots for the individual tasks are provided in appendix E.

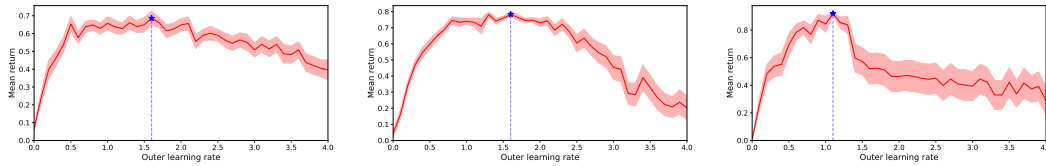


Figure 5: **Outer-LR hyperparameter sensitivity.** Mean normalized return across the Brax (left), Jumanji (center), MinAtar (right) tasks as a function of outer learning rate σ . Mean of 4 seeds plotted with standard error shaded. Normalized to task min/max across all experiments.

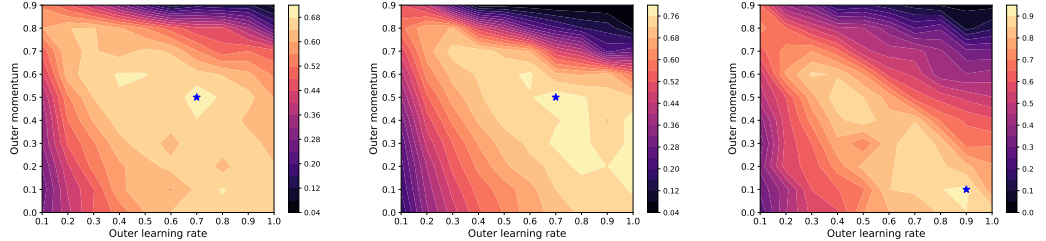


Figure 6: **Outer-Nesterov hyperparameter sensitivity.** Mean normalized return across the Brax (left), Jumanji (center), MinAtar (right) tasks as a function of outer learning rate σ and outer momentum μ . Mean of 4 seeds plotted. Normalized to task min/max across all experiments.

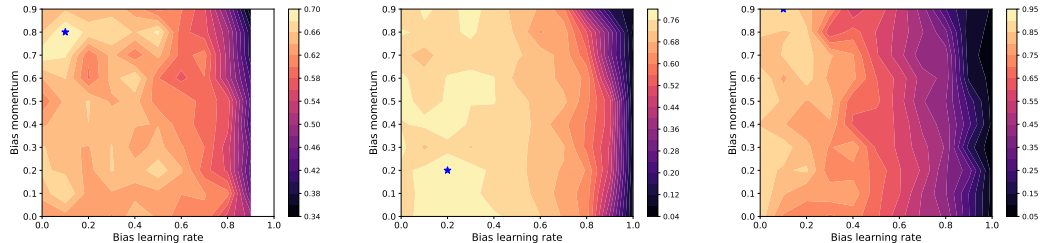


Figure 7: **Biased initialization hyperparameter sensitivity.** Mean normalized return across the Brax (left), Jumanji (center), MinAtar (right) tasks as a function of bias init learning rate α and bias momentum μ . Mean of 4 seeds plotted. Normalized to task min/max across all experiments.

Outer learning rate. When normalized across all tasks, Brax has low sensitivity to outer learning rate. The range of values $\sigma \in [0.8, 2.0]$ has comparable performance to the peak located at $\sigma = 1.6$. Notably, performance is not greatly reduced when using values up to $\sigma = 3.0$. Jumanji again exhibits near optimal-performance over a broad range of values $\sigma \in [0.5, 2.2]$, with the peak again located at $\sigma = 1.6$. Unlike in Brax, performance on Jumanji is greatly diminished for values $\sigma > 2.5$. MinAtar has a sharp peak in performance around standard PPO ($\sigma = 1.0$), with a rapid decrease in performance for values greater than this.

Nesterov. All three suites have a ridge-like trend in normalized performance, with poor performance where σ and μ are both small or both large. Both Brax and Jumanji have their peak at $(\sigma, \mu) = (0.7, 0.5)$, with a relatively broad plateau of near-optimal performance. The peak of MinAtar is at $(\sigma, \mu) = (0.9, 0.1)$, with a narrow ridge of near-optimal performance.

Biased initialization. The dominant trend on all three suites is decreasing normalized performance for large bias learning rate α . The optima for all suites at either $\alpha = 0.1$ (Brax, MinAtar) or $\alpha = 0.2$ (Jumajji). There is comparably little variation with respect to bias momentum μ , with the suite optima dispersed through the available range. Jumanji has a broader region of near optimal performance than Brax or MinAtar, covering $\alpha < 0.4$.

6 DISCUSSION

We now reflect on the questions posed in section 1. The PPO baselines in this work were tuned aggressively for each task, greatly increasing the confidence in the experimental findings. Given the baseline strength, and performance demonstrated in figures 3 and 4, we conclude in the *negative* for all three questions as evidenced by:

- Q1.** Varying the outer learning rate leads to a statistically significant increase on all point estimates on Brax and Jumanji, with corresponding increases to probability of improvement.
- Q2.** Employing Nesterov momentum on the outer loop, with outer learning rate attenuation, achieves statistically significant increases to all point estimates on Brax and Jumanji. We also observe a statistically significant probability of improvement on all three suites.
- Q3.** Momentum-biased initialization achieves statistically significant increase on all point estimates on Jumanji, with a probability of improvement of 0.6 on this suite.

Common hyperparameters. The sensitivity plots in figures 5, 6 demonstrate robust normalized performance across the Brax and Jumanji suites for outer-LR and outer-Nesterov. However, they do not indicate any significant increase in normalized return could be achieved over standard PPO for a set of common hyperparameters shared across a suite. To achieve the improved aggregate metrics in figure 3 it was necessary to use task-specific hyperparameters. We do however emphasize the aggressive, task-specific, tuning of the baseline, and view the robustness of normalized return across a range of hyperparameters as a strength of the methods.

Task-specific hyperparameters. Task-specific hyperparameter sensitivity plots are provided in appendix E. For outer-LR the optimal per-task values for α range between 0.5 (corresponding to cautious updates) and 2.3 (corresponding to confident updates). That values of α up to 2.3 can be optimal is surprising, as an α greater than unity directly violates the trust region established by our previous behavior policy. This precludes the provable monotonic improvement of PPO (Kuba et al., 2022); by stepping beyond the trust region we may in principle select a policy that is worse than the previous. For outer-Nesterov co-varying σ with μ can be understood through the effective learning rate $\sigma/(1 - \mu)$. The task-specific effective learning rate varies from 0.7 to 2.3. Lastly, for biased initialization the sharp peaks in performance on Brax tasks suggest the method suffers from high variance on this suite, hence the hyperparameters selected may not be optimal in expectation. On Jumanji the method is significantly less hyperparameter sensitive as evidenced by the smooth contours, providing an explanation for the performance gap observed between these suites.

MinAtar results. No outer-PPO method improved over baseline on MinAtar. We comment that other works committing substantial resources to baseline tuning on MinAtar have struggled to achieve improvements on the suite Jesson et al. (2023). Furthermore, the hyperparameter sensitivity plots in figures 5, 6 and 7 demonstrate all methods achieve peak normalized return greater than 0.9 on MinAtar. Since here we are normalizing to the maximum performing agents across all sweeps, this indicates there is less variance in the optimal performance of MinAtar compared to Brax and Jumanji with peak normalized returns around 0.7 and 0.8 respectively. A final explanation for the failure to surpass baseline on MinAtar could be ‘brittle’ base hyperparameters, not suited to the modified dynamics introduced by outer-PPO, supported by the sharp peak observed in outer-LR and concentration of performance in outer-Nesterov about standard PPO in figures 5 and 6.

Limitations. We identify two core limitations to this work; the *fixed transition budget* and the *lack of co-optimization* of base and outer-PPO hyperparameters. We only consider a timestep budget of 1×10^7 transitions. Whilst sample efficiency plots are provided in appendix D the hyperparameters have not been tuned to maximize performance in the data-limited regime. Furthermore, we do not consider the asymptotic performance for larger transition budgets, where it is possible the improvement achieved by outer-PPO methods may be diminished. With respect to co-optimization, given the dependence of the outer gradients on the base hyperparameters there is undoubtedly significant interaction between these and the outer-PPO hyperparameters. Exploring these interactions would yield better understanding and potentially improved performance. We additionally highlight the presence of learning rate annealing on the inner Adam instances in all experiments. This implies the outer gradients tend to zero, the implications of which we do not explore in this work.

7 RELATED WORK

The usage of the difference between initial parameters and those after gradient-based optimization as a ‘gradient’ has been explored for meta-learning in the Reptile algorithm (Nichol et al., 2018). Reptile aims to find an initialization that can be quickly fine-tuned across a distribution of tasks. Unlike outer-PPO, which applies this idea within a single RL task, Reptile performs gradient steps on different supervised learning tasks to determine the ‘Reptile gradient’. One could interpret outer-PPO as performing serial Reptile whereby each sampled task is the next PPO iteration alongside the collected dataset.

Whilst to the best of our knowledge we are the first to apply momentum to the outer loop of PPO, momentum-based optimizers such as RMSProp Tieleman & Hinton (2012) and Adam Kingma & Ba (2014) are commonly applied in other areas of RL. Recent work has examined the interaction of momentum based optimizers and RL objectives. Bengio et al. (2021) identify that a change in objective (such as by updating a target network or dataset), may lead to momentum estimates anti-parallel to the current gradient thereby hindering progress, and propose a correction term to mitigate this effect. Asadi et al. (2023) propose to reset the momentum estimates periodically throughout training and demonstrate improved performance on the Atari Learning Environment Bellemare et al. (2012) with Rainbow Hessel et al. (2017) doing so. However, none of these approaches focuses on PPO specifically, and instead address temporal difference learning or value based-methods.

Lastly, the biased initialization explored in this work is similar to the conjugate gradient initialization technique employed in hessian-free optimization Martens (2010), although this used only the prior iterate and not a momentum vector. Hessian-free optimization can be considered a supervised learning version of TRPO (Schulman et al., 2017a).

8 CONCLUSION

In this work, we introduced outer-PPO, a novel perspective of proximal policy optimization that applies arbitrary gradient-based optimizers to the outer loop of PPO. We posed three key research questions regarding the optimization process in PPO and conducted an empirical investigation across 14 tasks from three environments suites. Our experiments revealed that non-unity learning rates and momentum in the outer loop both yielded statistically significant performance improvements across a variety of evaluation metrics in the Brax and Jumanji environments, with gains ranging from 5-10% over a heavily tuned PPO baseline. Biased initialization provided improvements upon the baseline on Jumanji tasks but not Brax.

The most immediate direction for future research would be the exploration of interactions between base hyperparameters and outer-PPO hyperparameters. Since the optimal base hyperparameters may be unsuited to the modified dynamics of outer-PPO, the co-optimization of hyperparameters may yield performance improvements and deeper understanding of the method. Other possible future directions include the use of outer-PPO with alternatives to the clipped surrogate loss function, such as KL-penalized PPO Hsu et al. (2020) or discovered policy optimization Lu et al. (2022), and the use of adaptive optimizers on the outer loop such as RMSProp or Adam. Indeed, an ‘outer’ variant of many dual-loop RL algorithms can be defined, and we hope that this work will stimulate further research into optimizing RL algorithms through more sophisticated outer-loop strategies.

ACKNOWLEDGMENTS

This work was supported by a Turing AI World-Leading Researcher Fellowship G111021. Research supported with Cloud TPUs from Google’s TPU Research Cloud (TRC)

REFERENCES

- Rishabh Agarwal, Max Schwarzer, Pablo Samuel Castro, Aaron C Courville, and Marc Bellemare. Deep Reinforcement Learning at the Edge of the Statistical Precipice. In *Advances in Neural Information Processing Systems*, volume 34, pp. 29304–29320. Curran Associates, Inc., 2021. URL <https://proceedings.neurips.cc/paper/2021/hash/f514cec81cb148559cf475e7426eed5e-Abstract.html>. 6
- Marcin Andrychowicz, Anton Raichuk, Piotr Stańczyk, Manu Orsini, Sertan Girgin, Raphael Marinier, Léonard Hussenot, Matthieu Geist, Olivier Pietquin, Marcin Michalski, Sylvain Gelly, and Olivier Bachem. What Matters In On-Policy Reinforcement Learning? A Large-Scale Empirical Study, June 2020a. URL <http://arxiv.org/abs/2006.05990>. arXiv:2006.05990 [cs, stat]. 1, 6
- OpenAI: Marcin Andrychowicz, Bowen Baker, Maciek Chociej, Rafal Jozefowicz, Bob McGrew, Jakub Pachocki, Arthur Petron, Matthias Plappert, Glenn Powell, Alex Ray, et al. Learning dexterous in-hand manipulation. *The International Journal of Robotics Research*, 39(1):3–20, 2020b. 1
- Kavosh Asadi, Rasool Fakoor, and Shoham Sabach. Resetting the optimizer in deep rl: An empirical study. *arXiv preprint arXiv:2306.17833*, 2023. 10
- Marc G. Bellemare, Yavar Naddaf, Joel Veness, and Michael Bowling. The Arcade Learning Environment: An Evaluation Platform for General Agents. *Journal of Artificial Intelligence Research*, July 2012. doi: 10.1613/jair.3912. URL <https://arxiv.org/abs/1207.4708v2>. 10
- Emmanuel Bengio, Joelle Pineau, and Doina Precup. Correcting momentum in temporal difference learning. *arXiv preprint arXiv:2106.03955*, 2021. 10
- James Bergstra, Rémi Bardenet, Yoshua Bengio, and Balázs Kégl. Algorithms for Hyper-Parameter Optimization. In *Advances in Neural Information Processing Systems*, volume 24. Curran Associates, Inc., 2011. URL https://papers.nips.cc/paper_files/paper/2011/hash/86e8f7ab32cfd12577bc2619bc635690-Abstract.html. 6
- Christopher Berner, Greg Brockman, Brooke Chan, Vicki Cheung, Przemysław Dębniak, Christy Dennison, David Farhi, Quirin Fischer, Shariq Hashme, Chris Hesse, et al. Dota 2 with large scale deep reinforcement learning. *arXiv preprint arXiv:1912.06680*, 2019. 1
- Clément Bonnet, Daniel Luo, Donal John Byrne, Shikha Surana, Sasha Abramowitz, Paul Duckworth, Vincent Coyette, Laurence Illing Midgley, Elshadai Tegegn, Tristan Kalloniatis, Omayma Mahjoub, Matthew Macfarlane, Andries Petrus Smit, Nathan Grinsztajn, Raphael Boige, Cemyln Neil Waters, Mohamed Ali Ali Mimouni, Ulrich Armel Mbou Sob, Ruan John de Kock, Siddarth Singh, Daniel Furelos-Blanco, Victor Le, Arnun Pretorius, and Alexandre Laterre. Jumanji: a diverse suite of scalable reinforcement learning environments in JAX. In *The Twelfth International Conference on Learning Representations*, 2024. URL <https://openreview.net/forum?id=C4CxQmp9wc>. 2, 6
- Cédric Colas, Olivier Sigaud, and Pierre-Yves Oudeyer. Gep-pg: Decoupling exploration and exploitation in deep reinforcement learning algorithms. In *International conference on machine learning*, pp. 1039–1048. PMLR, 2018. 6
- Logan Engstrom, Andrew Ilyas, Shibani Santurkar, Dimitris Tsipras, Firdaus Janoos, Larry Rudolph, and Aleksander Madry. Implementation Matters in Deep Policy Gradients: A Case Study on PPO and TRPO, May 2020. URL <http://arxiv.org/abs/2005.12729>. arXiv:2005.12729 [cs, stat]. 1, 4, 6
- Daniel Freeman, Erik Frey, Anton Raichuk, Sertan Girgin, Igor Mordatch, and Olivier Bachem. Brax - A Differentiable Physics Engine for Large Scale Rigid Body Simulation. *Proceedings of the Neural Information Processing Systems Track on Datasets and Benchmarks*, 1, December 2021. URL <https://datasets-benchmarks-proceedings.neurips.cc/paper/2021/hash/d1f491a404d6854880943e5c3cd9ca25-Abstract-round1.html>. 2, 6

- Rihab Gorsane, Omayma Mahjoub, Ruan John de Kock, Roland Dubb, Siddarth Singh, and Arnu Pretorius. Towards a Standardised Performance Evaluation Protocol for Cooperative MARL. *Advances in Neural Information Processing Systems*, 35:5510–5521, December 2022. URL https://proceedings.neurips.cc/paper_files/paper/2022/hash/249f73e01f0a2bb6c8d971b565f159a7-Abstract-Conference.html. 6
- Matteo Hessel, Joseph Modayil, Hado van Hasselt, Tom Schaul, Georg Ostrovski, Will Dabney, Dan Horgan, Bilal Piot, Mohammad Azar, and David Silver. Rainbow: Combining Improvements in Deep Reinforcement Learning, October 2017. URL <http://arxiv.org/abs/1710.02298>. arXiv:1710.02298 [cs]. 10
- Chloe Ching-Yun Hsu, Celestine Mender-Dünner, and Moritz Hardt. Revisiting Design Choices in Proximal Policy Optimization, September 2020. URL <http://arxiv.org/abs/2009.10897>. arXiv:2009.10897 [cs, stat]. 1, 3, 4, 6, 10
- Andrew Jesson, Chris Lu, Gunshi Gupta, Angelos Filos, Jakob Nicolaus Foerster, and Yarin Gal. ReLU to the Rescue: Improve Your On-Policy Actor-Critic with Positive Advantages, November 2023. URL <http://arxiv.org/abs/2306.01460>. arXiv:2306.01460 [cs]. 9
- Sham M Kakade. A Natural Policy Gradient. In *Advances in Neural Information Processing Systems*, volume 14. MIT Press, 2001. URL <https://papers.nips.cc/paper/2001/hash/4b86abe48d358ecf194c56c69108433e-Abstract.html>. 3
- Diederik P Kingma and Jimmy Ba. Adam: A method for stochastic optimization. *arXiv preprint arXiv:1412.6980*, 2014. 6, 10, 14
- Jakub Grudzien Kuba, Christian Schroeder de Witt, and Jakob Foerster. Mirror Learning: A Unifying Framework of Policy Optimisation, July 2022. URL <http://arxiv.org/abs/2201.02373>. arXiv:2201.02373 [cs]. 1, 4, 9
- Chris Lu, Jakub Kuba, Alistair Letcher, Luke Metz, Christian Schroeder de Witt, and Jakob Foerster. Discovered Policy Optimisation. *Advances in Neural Information Processing Systems*, 35:16455–16468, December 2022. URL https://proceedings.neurips.cc/paper_files/paper/2022/hash/688c7a82e31653e7c256c6c29fd3b438-Abstract-Conference.html. 10
- James Martens. Deep learning via Hessian-free optimization. June 2010. URL <https://www.semanticscholar.org/paper/Deep-learning-via-Hessian-free-optimization-Martens/4c46347fbc272b21468efe3d9af34b4b2bad6684>. 6, 10
- Azalia Mirhoseini, Anna Goldie, Mustafa Yazgan, Joe Wenjie Jiang, Ebrahim Songhori, Shen Wang, Young-Joon Lee, Eric Johnson, Omkar Pathak, Azade Nazi, et al. A graph placement methodology for fast chip design. *Nature*, 594(7862):207–212, 2021. 1
- Volodymyr Mnih, Koray Kavukcuoglu, David Silver, Andrei A Rusu, Joel Veness, Marc G Belle-mare, Alex Graves, Martin Riedmiller, Andreas K Fidjeland, Georg Ostrovski, et al. Human-level control through deep reinforcement learning. *Nature*, 518(7540):529–533, 2015. 3
- Alex Nichol, Joshua Achiam, and John Schulman. On first-order meta-learning algorithms. *arXiv preprint arXiv:1803.02999*, 2018. 10
- John Schulman, Sergey Levine, Philipp Moritz, Michael I. Jordan, and Pieter Abbeel. Trust Region Policy Optimization, April 2017a. URL <http://arxiv.org/abs/1502.05477>. arXiv:1502.05477 [cs] version: 5. 1, 10
- John Schulman, Filip Wolski, Prafulla Dhariwal, Alec Radford, and Oleg Klimov. Proximal Policy Optimization Algorithms, August 2017b. URL <http://arxiv.org/abs/1707.06347>. arXiv:1707.06347 [cs]. 1, 3
- John Schulman, Philipp Moritz, Sergey Levine, Michael Jordan, and Pieter Abbeel. High-Dimensional Continuous Control Using Generalized Advantage Estimation, October 2018. URL <http://arxiv.org/abs/1506.02438>. arXiv:1506.02438 [cs]. 3

- David Silver, Julian Schrittwieser, Karen Simonyan, Ioannis Antonoglou, Aja Huang, Arthur Guez, Thomas Hubert, Lucas Baker, Matthew Lai, Adrian Bolton, et al. Mastering the game of go without human knowledge. *nature*, 550(7676):354–359, 2017. 3
- Ilya Sutskever, James Martens, George Dahl, and Geoffrey Hinton. On the importance of initialization and momentum in deep learning. In *International conference on machine learning*, pp. 1139–1147. PMLR, 2013. 5
- Tijmen Tieleman and Geoffrey Hinton. Lecture 6.5-rmsprop: Divide the gradient by a running average of its recent magnitude. *COURSERA: Neural networks for machine learning*, 4(2):26–31, 2012. 10
- Edan Toledo. Stoix: Distributed single-agent reinforcement learning end-to-end in jax, 2024. URL <https://github.com/EdanToledo/Stoix>. 14
- Shuhei Watanabe. Tree-Structured Parzen Estimator: Understanding Its Algorithm Components and Their Roles for Better Empirical Performance, May 2023. URL <http://arxiv.org/abs/2304.11127>. arXiv:2304.11127 [cs]. 6
- Kenny Young and Tian Tian. MinAtar: An Atari-Inspired Testbed for Thorough and Reproducible Reinforcement Learning Experiments, June 2019. URL <http://arxiv.org/abs/1903.03176>. arXiv:1903.03176 [cs]. 2, 6

A FURTHER DETAILS ON PPO

A.1 INNER OPTIMIZATION LOOP

Algorithm 6 PPO Inner Optimization Loop

```

1: Input:  $\theta$  (initial parameters),  $\mathcal{D}$  (collected trajectories),  $\hat{A}$  (estimated advantages)
2:  $\theta^\pi, \theta^V \leftarrow \theta$ 
3: for epoch  $i = 1, 2, \dots, N$  do
4:   Shuffle  $(\mathcal{D}, \hat{A})$  and create  $M$  minibatches  $\{(\mathcal{D}_1, \hat{A}_1), (\mathcal{D}_2, \hat{A}_2), \dots, (\mathcal{D}_M, \hat{A}_M)\}$ 
5:   for  $j = 1, 2, \dots, M$  do
6:      $\theta^\pi \leftarrow \theta^\pi + \eta \nabla_{\theta^\pi} L^\pi(\theta^\pi, \mathcal{D}_j, \hat{A}_j)$ 
7:      $\theta^V \leftarrow \theta^V + \eta \nabla_{\theta^V} L^V(\theta^V, \mathcal{D}_j, \hat{A}_j)$ 
8:   end for
9: end for
10:  $\theta \leftarrow \theta^\pi, \theta^V$ 
11: Return:  $\theta^* \leftarrow \theta$ 

```

Algorithm 6 describes the inner optimization loop of proximal policy optimization, where L^π and L^V are defined in equations 1 and 4 respectively. For notational ease this presentation is slightly simplified. Typically, instead of the gradient ascent steps taken in lines 5 and 6 typically each of θ^π and θ^V are optimized using independent instances of Adam (Kingma & Ba, 2014), with potentially distinct learning rates $\eta^\pi \neq \eta^V$.

A.2 CLIPPED VALUE OBJECTIVE

$$L^V(\theta^V) = \max \left[(V_{\theta_k} - V_{\text{targ}})^2, (\text{clip}(V_{\theta_k}, V_{\theta_{k-1}} - \varepsilon, V_{\theta_{k-1}} + \varepsilon) - V_{\text{targ}})^2 \right] \quad (4)$$

B IMPLEMENTATION DETAILS

We implement our experiments using the JAX-based Stoix library (Toledo, 2024). Our implementation is such that several seeds can be trialed / evaluated simultaneously for the same hyperparameters using a single device. We used Google Cloud TPU (v4-8) for these experiments. The runtime varied between environments, and given different hyperparameters (e.g parallel environments, rollout length, batch size, number of inner epochs) with an average of approximately 10 minutes per 4-seed trial.

C HYPERPARAMETERS

C.1 SWEEP RANGES

The sweep ranges for baseline hyperparameter sweeps are presented in table 1.

Table 1: Sweep ranges for baseline hyperparameters.

Parameter	Sweep Range
Parallel environments	2^6 to 2^{10}
Rollout	2^2 to 2^8
Num. epoch	1 to 16
Num. minibatch	2^0 to 2^6
Actor learning rate	1×10^{-5} to 1×10^{-3} (log scale)
Critic learning rate	1×10^{-5} to 1×10^{-3} (log scale)
Discount factor (γ)	0.9 to 1.0
GAE λ	0.0 to 1.0
Clip ϵ	0.1 to 0.5
Max gradient norm	0.1 to 5.0
Reward scaling	0.1 to 100 (log scale)

C.2 OPTIMAL VALUES

The optimal values identified by the baseline sweep, up to trial 500, are included in table 2. These values are the ‘base’ hyperparameters used for outer-PPO methods.

Table 2: Optimal values from baseline sweep up to trial 500

Task	Parallel env.	Rollout	Num. epoch	Num. m-batch	Actor lr	Critic lr	Discount γ	GAE λ	Clip ϵ	Max g. norm	Reward scale
ant	128	8	2	32	3.0e-04	1.4e-04	0.98	0.70	0.21	4.85	0.14
halfcheetah	64	64	3	16	3.9e-04	4.4e-04	0.99	0.94	0.13	2.40	0.46
hopper	64	64	2	64	6.3e-04	3.6e-04	1.00	0.96	0.17	3.54	3.95
humanoid	256	64	4	64	1.0e-04	1.0e-04	0.98	0.89	0.34	3.30	0.14
humanoidstandup	64	64	3	32	3.0e-04	8.2e-04	0.99	0.98	0.10	4.65	0.35
walker2d	256	32	4	64	5.4e-04	8.2e-04	1.00	0.92	0.12	3.74	22.54
asterix	128	128	3	64	8.3e-04	2.1e-05	1.00	0.20	0.30	2.28	6.62
breakout	64	16	14	16	1.8e-04	1.2e-04	0.90	0.53	0.16	0.25	5.19
freeway	64	128	10	2	6.9e-04	1.3e-04	0.98	0.70	0.15	4.71	6.64
space_invaders	128	32	16	2	3.0e-05	1.1e-04	0.98	1.00	0.25	0.35	0.61
game_2048	1024	8	9	32	4.9e-04	3.8e-04	0.99	0.04	0.28	2.56	0.13
maze	256	32	7	64	6.5e-04	4.3e-04	0.98	0.66	0.14	2.46	1.97
rubiks_cube	64	256	13	4	9.0e-04	2.2e-04	0.99	0.55	0.14	3.45	11.03
snake	1024	8	11	4	6.0e-04	6.0e-04	1.00	0.46	0.12	2.52	20.48

Table 3: Optimal hyperparameters per task for each outer-PPO method

Task	Outer-LR	Outer-Nesterov		Biased Initialization	
	σ	σ	μ	α	μ
Ant	0.5	0.7	0.2	0.1	0.8
HalfCheetah	0.5	0.4	0.5	0.2	0.8
Hopper	1.5	0.9	0.4	0.5	0.8
Humanoid	1.9	0.5	0.7	0.1	0.4
HumanoidStandup	2.1	0.5	0.3	0.5	0.8
Walker2d	2.0	0.9	0.6	0.4	0.0
2048	1.3	0.8	0.4	0.3	0.9
Snake	2.3	1.0	0.4	0.7	0.5
Rubik’s Cube	1.7	0.5	0.7	0.4	0.3
Maze	0.9	0.9	0.0	0.1	0.5
Asterix	1.1	0.6	0.5	0.1	0.4
Breakout	1.1	0.9	0.1	0.0	0.5
Freeway	1.6	0.9	0.3	0.2	0.5
Space Invaders	1.3	0.8	0.2	0.1	0.9

D ADDITIONAL RESULTS

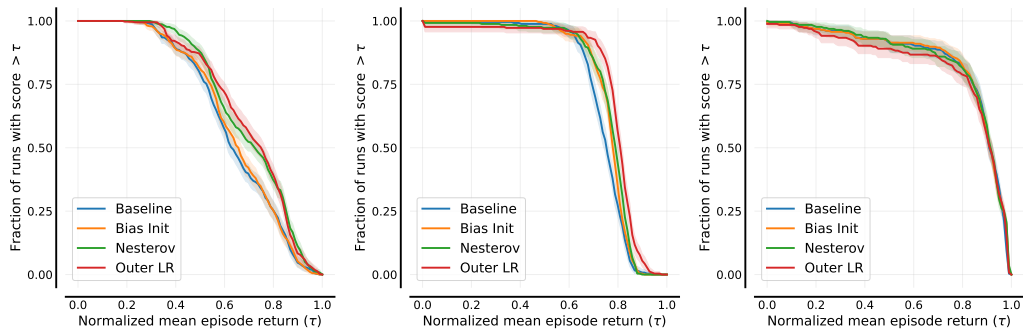


Figure 8: **Performance profiles for Brax (left), Jumanji (center), and MinAtar (right).** 6 / 4 / 4 tasks used from Brax / Jumanji / MinAtar respectively. For each task, agents are trained and evaluated using 64 seeds.

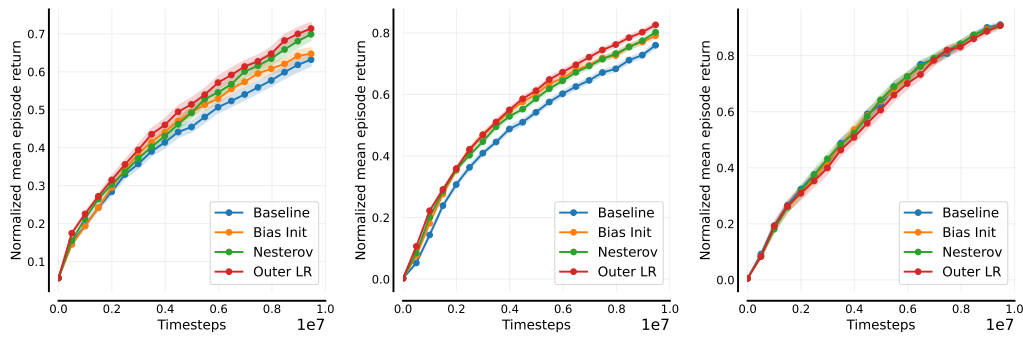


Figure 9: Sample efficiency curves for Brax (left), Jumanji (center), and MinAtar (right).

Table 4: Minimum and maximum returns used for normalization.

Task	Min	Max
Ant	-2958.14	13466.48
Halfcheetah	-587.37	7859.28
Hopper	21.03	3697.39
Humanoid	207.63	11851.71
Humanoidstandup	6686.00	71897.67
Walker2d	-32.44	2558.61
2048	989.50	29084.63
Snake	0.00	92.55
Rubiks Cube	0.00	0.66
Maze	0.03	0.84
Asterix	0.30	64.46
Breakout	0.00	92.86
Freeway	0.00	66.13
Space Invaders	0.00	191.80

E SWEEP PERFORMANCES

E.1 BASELINE

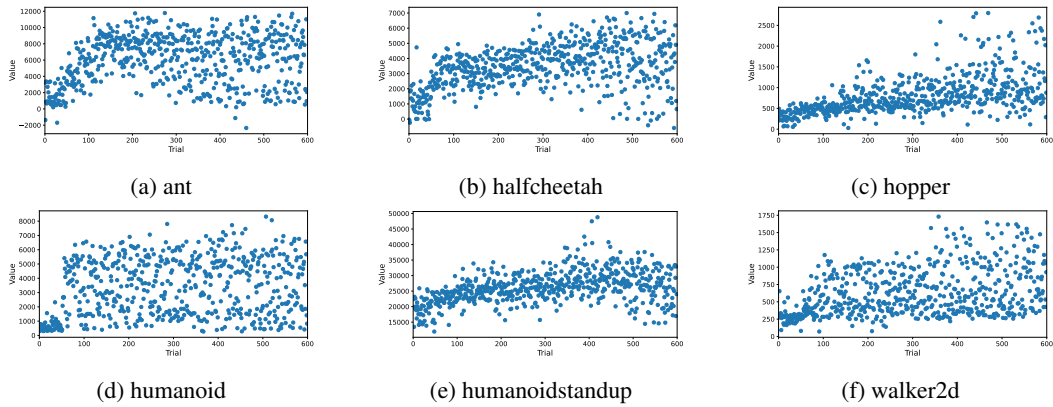


Figure 10: **Baseline sweep performance for Brax tasks.** Each point represents the mean of a 4 seed trial.

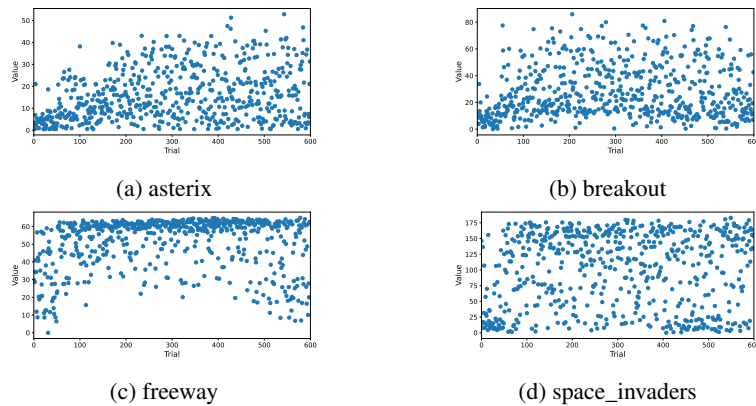


Figure 11: **Baseline sweep performance for MinAtar tasks.** Each point represents the mean of a 4 seed trial.

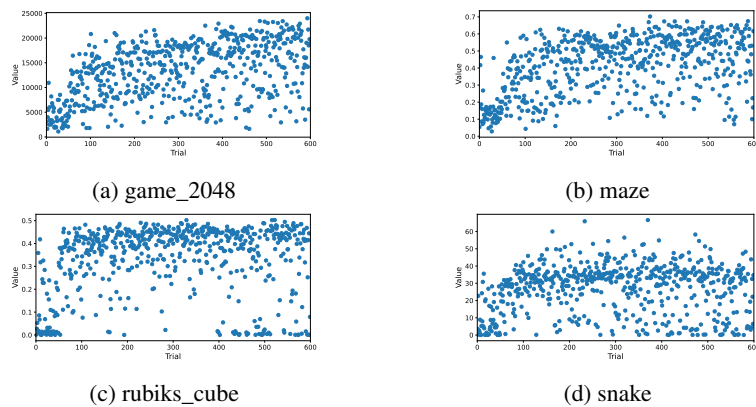


Figure 12: **Baseline sweep performance for Jumajji tasks.** Each point represents the mean of a 4 seed trial.

E.2 OUTER LEARNING RATES

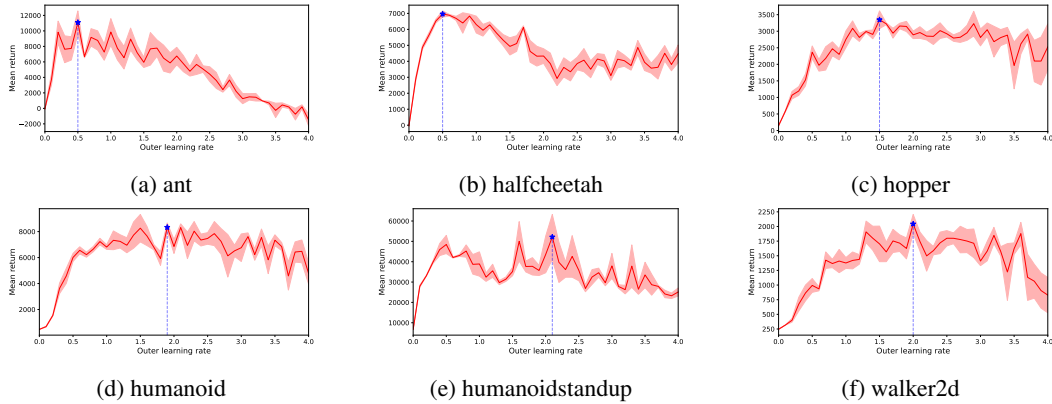


Figure 13: **Outer learning rate sweep performance for Brax tasks.** Mean of 4 seeds shown with standard error shaded. Optimal point marked with blue star.

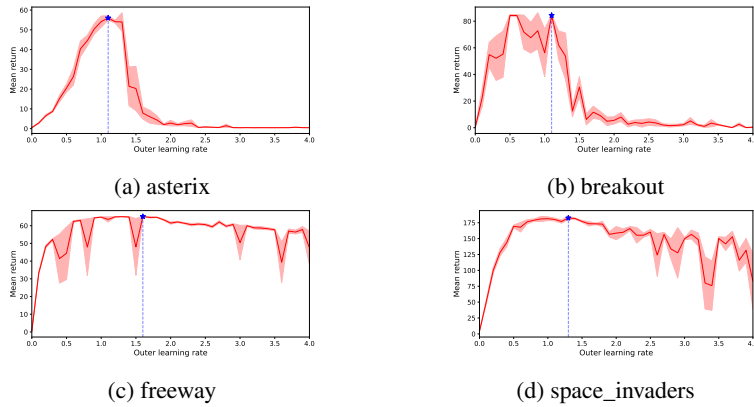


Figure 14: **Baseline sweep performance for MinAtar tasks.** Mean of 4 seeds shown with standard error shaded. Optimal point marked with blue star.

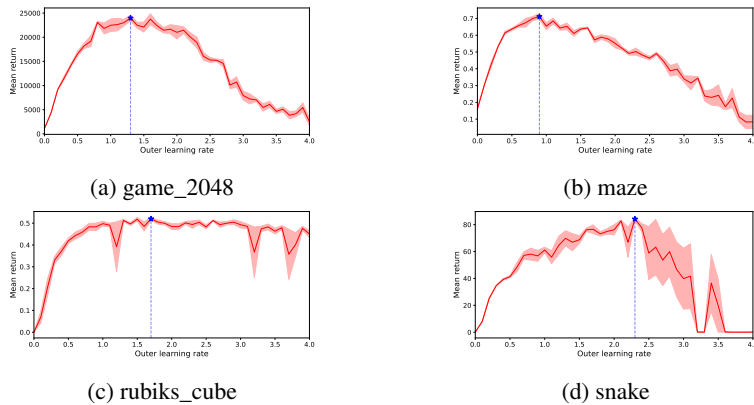


Figure 15: **Baseline sweep performance for Jumajji tasks.** Mean of 4 seeds shown with standard error shaded. Optimal point marked with blue star.

E.3 NESTEROV MOMENTUM

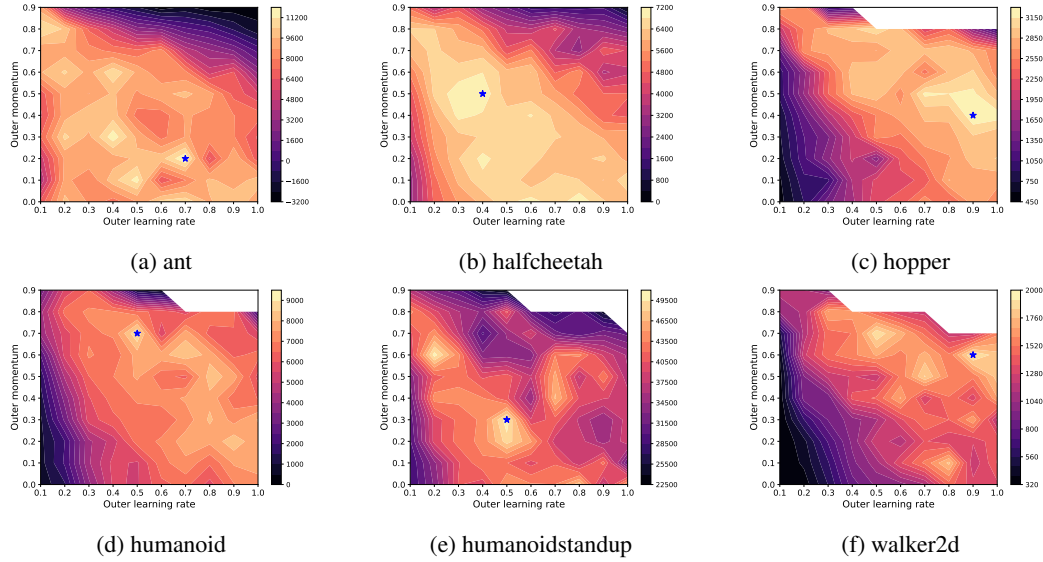


Figure 16: **Nesterov sweep performance for Brax tasks.** Contour plot of mean of 4 seeds. White regions resulted in numerical errors (NaN). Optimal point marked with blue star.

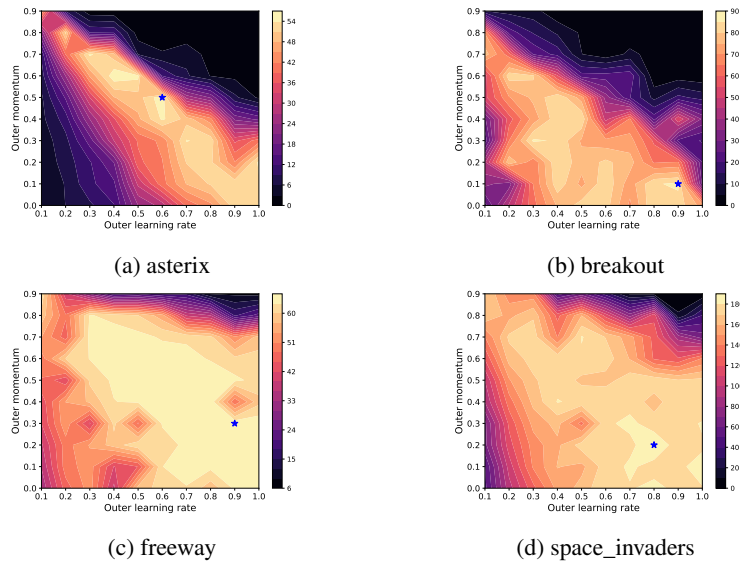


Figure 17: **Nesterov sweep performance for MinAtar tasks.** Contour plot of mean of 4 seeds. White regions resulted in numerical errors (NaN). Optimal point marked with blue star.

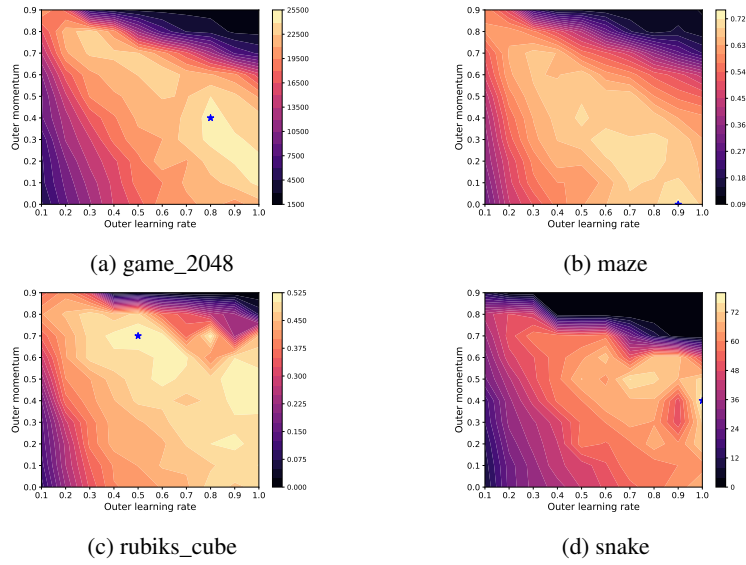


Figure 18: **Nesterov sweep performance for Jumanji tasks.** Contour plot of mean of 4 seeds. White regions resulted in numerical errors (NaN). Optimal point marked with blue star.

E.4 BIASED INITIALIZATION

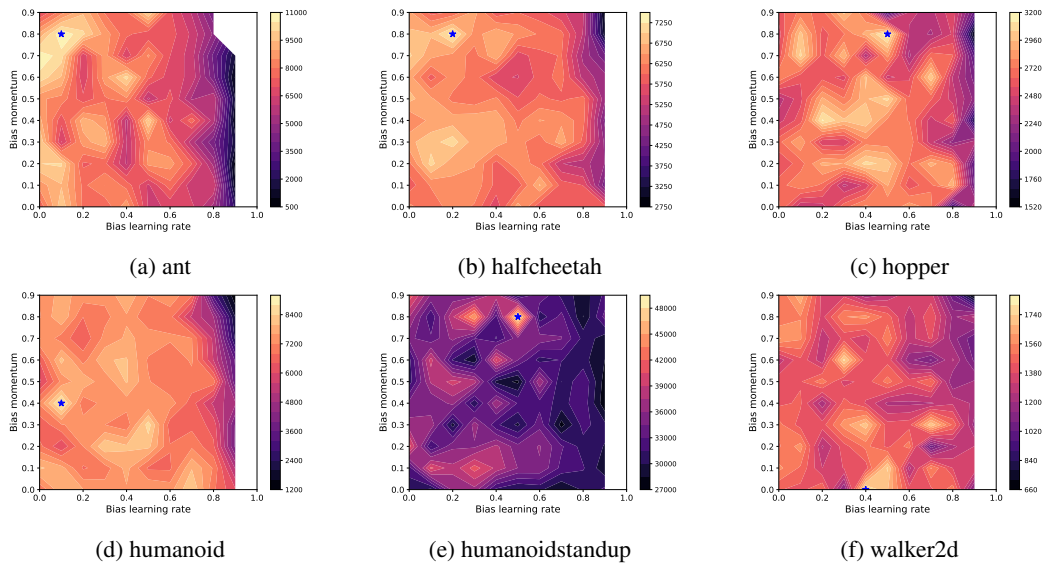


Figure 19: **Biased initialization sweep performance for Brax tasks.** Contour plot of mean of 4 seeds. White regions resulted in numerical errors (NaN). Optimal point marked with blue star.

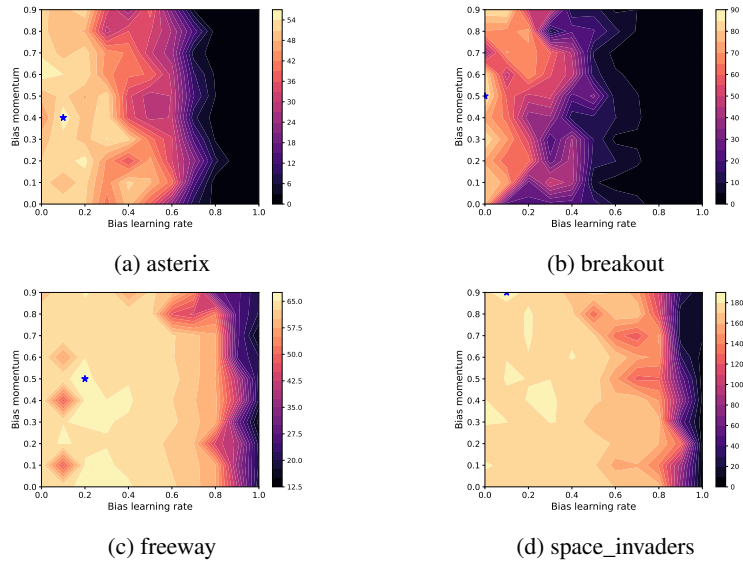


Figure 20: **Biased initialization sweep performance for MinAtar tasks.** Contour plot of mean of 4 seeds. White regions resulted in numerical errors (NaN). Optimal point marked with blue star.

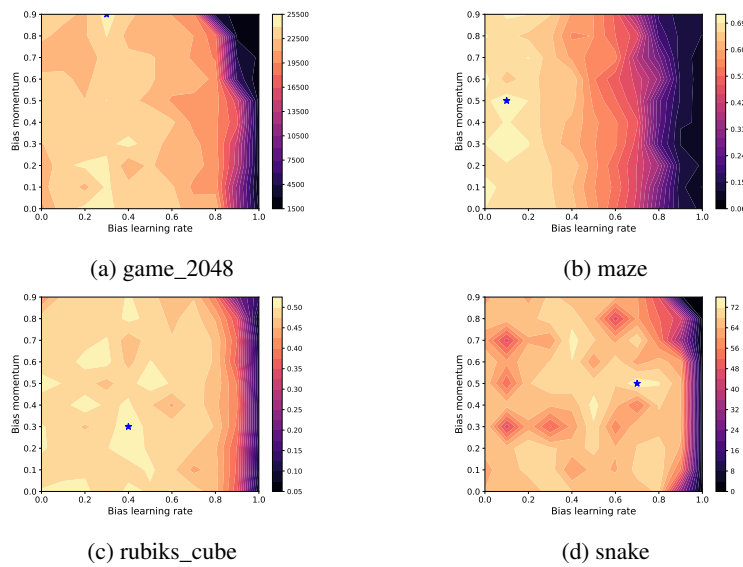


Figure 21: **Biased initialization sweep performance for Jumanji tasks.** Contour plot of mean of 4 seeds. White regions resulted in numerical errors (NaN). Optimal point marked with blue star.

F INDIVIDUAL TASK PERFORMANCES

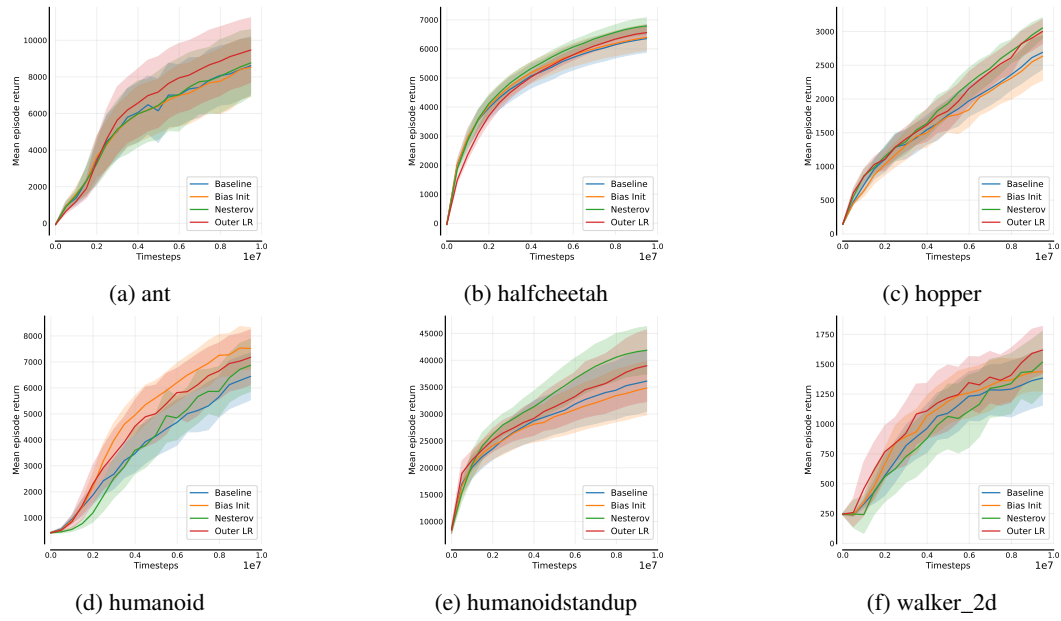


Figure 22: **Individual task performance for Brax.** For each task mean of 64 seeds is presented with standard deviation shaded.

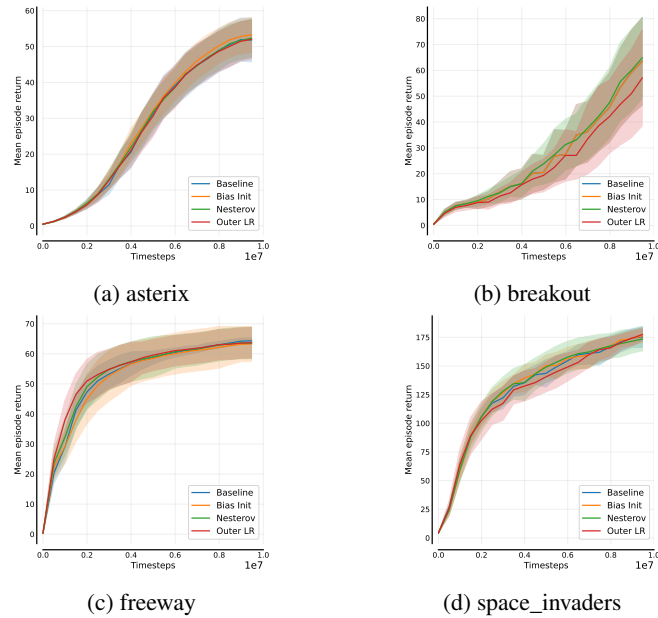


Figure 23: **Individual task performance for MinAtar.** For each task mean of 64 seeds is presented with standard deviation shaded.

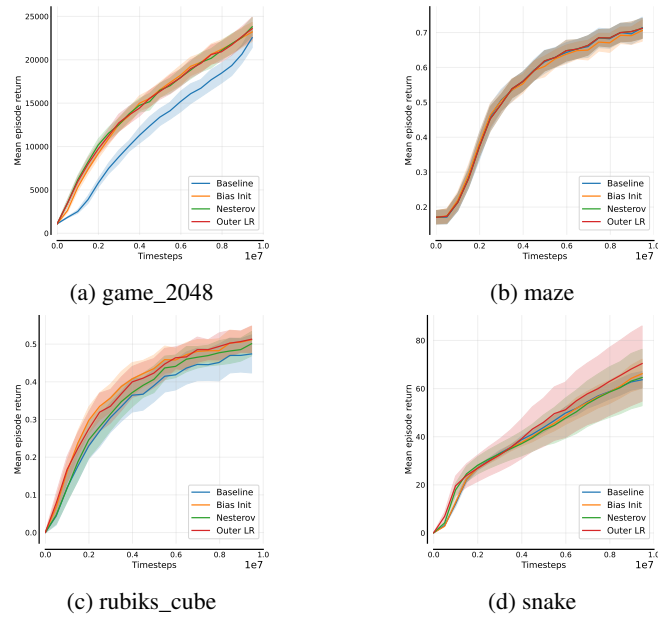


Figure 24: **Individual task performance for Jumanji.** For each task mean of 64 seeds is presented with standard deviation shaded.